國 立 交 通 大 學

材料科學與工程學系

碩 士 論 文

以陽離子交換法合成硒化物奈米棒

Synthesis of Selenide Nanorods through Cation Exchange Reaction

研 究 生：Thi An Nguyen

指導教授：徐雍鎣 博士

中 華 民 國 九十九 年 七 月

Synthesis of Selenide Nanorods through Cation Exchange Reaction

Student: Thi An Nguyen Advisor: Dr. Yung-Jung Hsu

National Chiao Tung University

Department of Materials Science and Engineering

ABSTRACT:

In the present work, we have successfully synthesized a variety of selenides nanorods including CdSe, ZnSe and some $Cd_{1-x}Zn_xSe$ alloys through a cation exchange approach. The growth mechanism for these selenide nanorods was also studied, compared, and discussed. In the typical process, single crystalline nanorods of Se were first synthesized through a carboxylmethyl cellulose-assisted chemical reduction approach. A direct incorporation of Ag^+ into Se nanorods was then conducted by the addition of $AgNO_3$ into the Se nanorods solution, resulting in the formation of Ag_2Se nanorods. Further replacement of Ag^+ of Ag_2Se nanorods with Cd^{2+} and Zn^{2+}can be achieved by the cation exchange reactions, leading to the growth of single-crystalline CdSe, and ZnSe nanorods, respectively. The as-synthesized selenides nanorods have diameters of 50-70 nm and lengths varying from 500-800 nm, similar to those

of the starting Se nanorods. By using this method in our experiment, we may further obtain ternary alloyed selenide nanorods, for example, $Cd_{1-x}Zn_xSe$, to study the effect of cation composition on the resulting in optical properties of nanorods. The present synthetic approach can be readily applied to prepare other selenide- and sulfide-based nanostructures.

以陽離子交換法合成硒化物奈米棒

學生：Thi An Nguyen　　　　指導教授：徐雍鎣 博士

國立交通大學

材料科學與工程學系

中文摘要:

在此篇論文中我們成功地合成出多種不同成分之單晶硒化物奈米棒，例如:CdSe、ZnSe，且利用陽離子交換法合成出 $Cd_{1-x}Zn_xSe$ 奈米棒。而在此也將討論研究和比較各種奈米棒之成長機制。透過一個典型的製程可以成功利用纖維素輔助之化學還原法合成出單晶硒奈米棒，且將 Ag^+ 離子直接加入硒奈米棒水溶液中,即可直接獲得高產率之 Ag_2Se 奈米棒。接著透過陽離子置換法可將 Ag_2Se 中之 Ag^+ 離子分別地換成 Zn^{2+} 離子和 Cd^{2+} 離子，而得到單晶結構之 ZnSe 和 CdSe 奈米棒。利用此法合成出之硒化物奈米棒直徑約 50-70nm 且長度分佈在 500-800，非常相近於起始之硒奈米棒。更進一步的利用陽離子交換法可以合成出三元之硒化物奈米棒，如 $Cd_{1-x}Zn_xSe$，且其成分之控制和其光學性質也在此篇論文被探討研究。此合成之方法可以簡單應用在製備各類之硒化物和硫化物之奈米結構。

ACKNOWLEDGMENT

The completion of the Master’s degree and of the Master’s thesis was not done without the support of others. I needed guidance, ideas, challenges and encouragement of many to be successful. I was lucky enough to receive this kind of aid from many sources.

First of all, I would like to express my deepest gratitude to my advisor, Dr. Hsu Yung-Jung, who helped me a lot for completing the thesis and showed me again that encouragement and pushes can be fantastic motivating tools. He has offered me valuable ideas, suggestions and criticisms in rich research experience. His patience and kindness are greatly appreciated.

Secondly, I wish to extend my thanks to the Department of Materials and Engineering, for their support of this study, especially those who helped me on the journey toward the completion of my thesis.

Thirdly, I appreciate all the input that I received from my lab-mates. I learned a lot from everyone that I worked with during the program. Thanks are also due to my graduate friends, who never failed to give me great encouragement and suggestions.

Finally, I would like to thank my family for their support all the way from the very beginning of my postgraduate study. I am thankful to all my family members for their thoughtfulness and encouragement.

Those experiences enriched my life. I will try to take knowledge and the friendships with me wherever I go. Thank you for all your help and guidance.

Table of Content

Figures and Captions

I. INTRODUCTION

1. Properties of CdSe, ZnSe II-VI Semiconductor

Cadmium Selenide (CdSe) is a semiconducting material with a direct bandgap of about 1.74 eV. This material is transparent to infra-red (IR) light, and has been widely used in windows for instruments utilizing IR light. Researchers are concentrating on developing controlled syntheses of CdSe nanocrystals. In addition to synthesis, scientists have been working to understand the properties of CdSe, as well as apply these materials in useful ways.[1, 2]

Three crystalline forms of CdSe are known: wurtzite (hexagonal), sphalerite (cubic) and rock-salt (cubic). The sphalerite CdSe structure is unstable and converts to the wurtzite form upon moderate heating. The rock-salt structure is only observed under high pressure. CdSe in its wurtzite crystal structure is an important II-VI semiconductor. CdSe is an n-type semiconductor, which is difficult to be doped to become p-type. CdSe is being developed for use in opto-electronic devices, laser diodes, nanosensing, and biomedical imaging.[3-7] They are also tested for use in high-efficiency solar cells. CdSe nanorods are interesting for photovoltaic applications since the long axis of the rod provides a continuous channel for transporting electrons. To use nanorods in a practical application, surface functionalization is usually explored to control their lateral distribution and positional orientation. [8, 9]

Zinc Selenide (ZnSe) is a light yellow binary solid compound. It is an intrinsic semiconductor with a band gap of about 2.70 eV at 25 °C and it emits blue light. ZnSe is used to form II-VI light-emitting diodes and diode lasers. It is susceptible to n-type after doped with, for example, halogen elements. P-type doping is more difficult, but can be achieved by introducing nitrogen. In daily life, it can be found as the entrance optic in the new range of "in-ear" clinical thermometers and can be just seen as a small yellow window. ZnSe can slowly react with atmospheric moisture, but this is not generally a serious problem. Panda et al described a chemical route for the synthesis of size-, shape-, and phase-controlled ZnSe nanocrystals with dimensions below the Bohr radius. [10] ZnSe nanorods and nanowires can be synthesized in a hot-injection process by varying the ratios of ligand solvents, TOPO and ODA at relatively low temperature.

2. Studies of CdSe and ZnSe 1-D Nanocrystals

The unique optical and electrical properties of one-dimensional (1-D) semiconductor nanostructures, such as nanorods and nanowires, can be exploited for use in a number of applications, including solar cells, photonic crystals, lasers, transistors, and sensors. Quantum dots are attractive for both electronic materials applications, for example, as light-emitting diodes,[6, 13] and for biotechnology, for examples, as fluorescence tags in diagnostics.[14] Nanorods may be more advantageous, as the long axis of the nanorods provides a continues pathway for electron transport. One-dimensional nanostructures have received ever-growing interest because of their fascinating properties and unique applications that cannot be obtained from nanoparticles or bulk solids. The various 1-D nanostructures (nanorods, nanowires, nanobells, nanotubes) thus represent ideal systems for dimension-dependent optical, electrical, and mechanical properties and are expected to play an important role as building blocks in relevant devices and processes.[3-5, 7-8, 11, 15]

Lots of synthetic methods for preparing controlled size and shape of 1-D nanostructures based on physical and chemical approaches have been developed, including hydrothermal methods, microwave irradiation, sequential reactant injection, solvothermal methods, self-assembly, template-assisted, and seeded-type approaches.[16-21] Talapin et al successfully synthesized layered colloidal crystals of CdSe nanorods by slow destabilization of a nanocrystal solution upon allowing the diffusion of a nonsolvent into the colloidal solution of nanocrystals.[19] The organization of semiconductor nanorods into ordered 3-D superstructures were observed for the first time. The proposed self-assembly technique is shown to be applicable to arrange nanorod materials in large scale.

3. Studies of $Cd_{1-x}Zn_xSe$ Alloyed Nanocrystals

The development in the field of synthesis of semiconductor nanocrystals aims at the use of easy-to-manipulate and inexpensive methods that can even be applied to industrial scaling. Such methods have been reported recently, for example, for the preparation of CdSe, CdS, CdTe, ZnSe nanocrystals. However, some drawbacks exist in these binary nanocrystals, for example, low quantum yield and limitation of emission region. Therefore, alloying two materials to form ternary nanocrystals such as $Cd_{1-x}Zn_xSe$ (E = Se, or S) become the subject of this field. The ternary semiconductor nanocrystals may emit colors with tunable wavelength via the variation of the compositions.[22-27] The luminescence properties of the ternary alloyed nanocrystals are comparable to or even better than their binary counterparts.

$Cd_{1-x}Zn_xSe$ alloyed nanocrystals are attractive materials for luminescence since their emission color can be tuned from the UV/blue region (ZnSe) to the visible (CdSe) by changing the composition, that is, the Cd:Zn ratio, without changing the nanocrystal size. Most of the $Cd_{1-x}Zn_xSe$ alloyed quantum dots reported in literature were prepared through the organometallic method and exhibited quantum yields above 45%.[26] In the previous study, $Cd_{1-x}Zn_xSe$ alloyed nanocrystals were prepared via the direct incorporation of Zn^{2+} and Se^{2-} ions into the pre-synthesized CdSe nanocrystals at high temperature.[37] As the starting CdSe nanocrystals have the large size, the resulting alloyed nanocrystals were with the emission wavelength longer than 490 nm. The use of very small ZnSe and CdSe particles as initial seeds can result in the formation of alloyed nanocrystals with shorter emission wavelength.

Figure 1.1 shows the PL and absorption spectra for the $Cd_{1-x}Zn_xSe$ nanocrystals with various Zn molar fractions of 0, 0.28, 0.44, 0.55, and 0.67. In the absorption spectra, the first excitonic absorption wavelength of CdSe was quenched with the incorporation of ZnSe, while the overall shape remained similar. With the increase of the Zn fraction from 0 to 0.67, a significant blue-shift of about 110-120 nm was observed for both the first excitonic absorption onset and the band-edge luminescence peak of the nanocrystals.

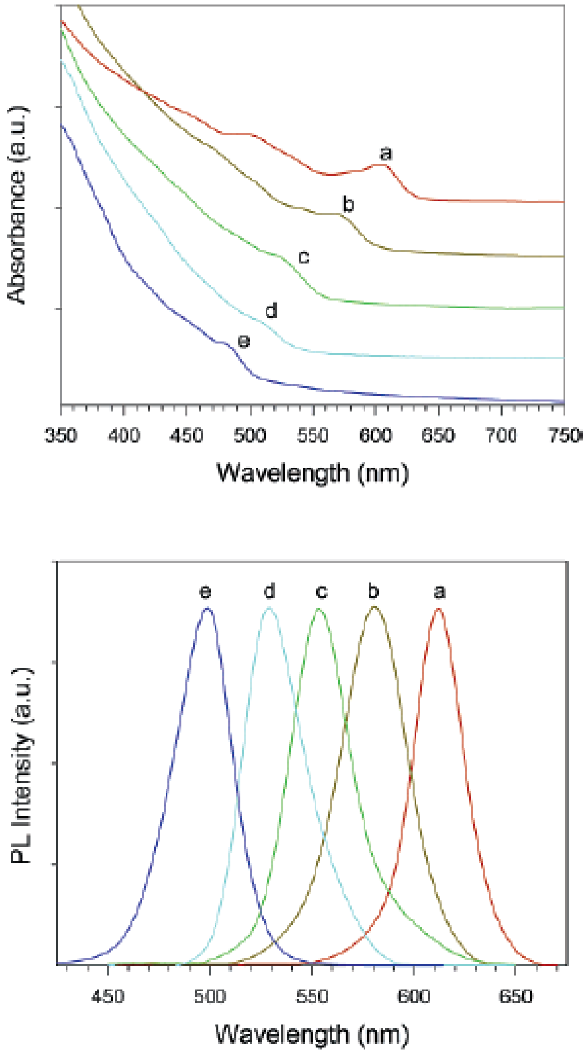

Figure 1.1: Absorption (top) and PL spectra with λ_{ex}=365 nm (bottom) for the $Cd_{1-x}Zn_xSe$ nanocrystals with Zn fractions of (a) 0, (b) 0.28, (c) 0.44, (d) 0.55, and (e) 0.67.[27]

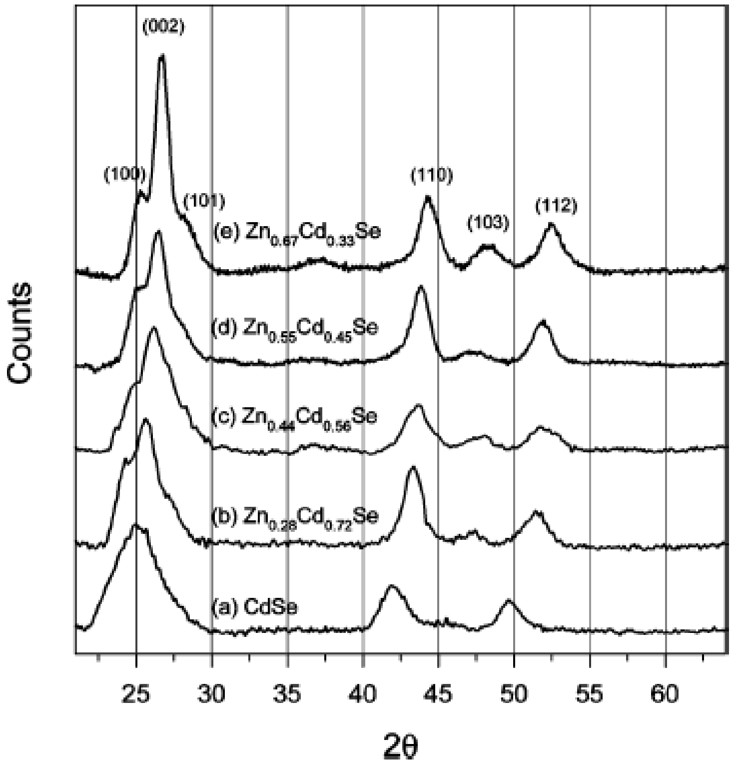

Figure 1.2: X-ray powder diffraction patterns of $Cd_{1-x}Zn_xSe$ nanocrystals with Zn fractions of (a) 0, (b) 0.28, (c) 0.44, (d) 0.55, and (e) 0.67.[27]

The X-ray diffraction analysis may provide us with useful information to confirm the alloy composition in the nanocrystals. As shown in Figure 1.2, the diffraction peaks of nanocrystals gradually shifted toward high 2θ regions as the Zn content was increased. This phenomenon can be realized by the fact that the replacement of Cd with Zn of smaller atomic size in alloyed nanocrystals may lead to the shrinkage in unit cell and thus the decrease in lattice spacing. As a result, the alloyed $Cd_{1-x}Zn_xSe$ nanocrystals showed diffraction peaks at higher 2θ regions as compared to the pure CdSe.

4. Cation Exchange Reaction

Ion exchange is an exchange of ions between two electrolytes or between an electrolyte solution and a complex. Ion exchangers are either cation exchangers that exchange positively charged ions (cations) or anion exchangers that exchange negatively charged ions (anions). Cation exchange reactions have been demonstrated as useful and simple methods for preparing thin films and nanocrystals with specific composition.[29-36] The conversion reaction is kinetically prohibited at ambient conditions in the bulk due to the high activation energy required for the diffusion of ions in the solid lattice framework. Nevertheless, the activation energy decreases as particle size decreases, enabling exchange to occur within seconds for nanoparticles. Cation exchange provides a facile method for systematically varying the proportion of two chemical compositions within a single nanocrystal and studying its effect. In the present work, we successfully demonstrated that cation exchange can be used to completely convert Ag_2Se nanorods to CdSe, ZnSe and $Cd_{1-x}Zn_xSe$ alloyed nanorods. More importantly, the conversion process could be reversibly performed.

The large difference in solubility product (K_{sp}) is a key factor toward direct replacement between two kinds of cations. Nanocrystals can spontaneously be converted into the other composition with smaller K_{sp}. For instance, several cations including Cu^{+}, Ag^{+}, Sb^{3+}, and Bi^{3+} have been used to replace Zn^{2+} in ZnS nanotubes to produce the corresponding sulfides with the preservation of the tubular shape.[28] This approach opens up a new access to design and prepare nanostructures that are difficult to be obtained through the general methods.

For the synthesis of chalcogenide semiconductors, the cation exchange has been used in most studies, whose crystal structures are determined by frameworks of the chalcogen anions (S^{2-}, Se^{2-}, Te^{2-}).[30-36] The metal cations are relatively mobile in the anionic framework, making it possible to replace the cations under moderate reaction conditions. It is believed that this chemical transformation is different from the Kirkendall effect caused by the difference in diffusion flux between two chemical species.

In 2004 Alivisatos et al first reported a research about the cation exchange reaction for nanocrystal synthesis.[29] They found some interesting phenomena about the reversible transformation between CdSe and Ag_2Se nanocrystals. CdSe could be transformed into Ag_2Se easily by the addition of

Ag^{+} due to thermodynamically favorable regime. Note that the reverse transformation (from Ag_2Se to CdSe) was thermodynamically forbidden. Such conversion however can be achieved through a kinetically controlled approach, in which a large amount of Cd^{2+} and the reaction initiator (TBP, tri-butyl phosphate) were necessarily added in the growth.

Figure 1.3 shows TEM images of the initial CdSe nanorods of different sizes and their transformed Ag_2Se nanocrystals. It is apparent that thinner nanorods (Figure 1.3A) reorganized to spherical shape during the forward reaction, which indicates that the anion sublattice was completely disrupted during the reaction (Figure 1.3B). The dependence of width and the length of initial nanorods on the morphology of the product suggested that nanorod thickness is more relevant to the shape change in the resulting product.

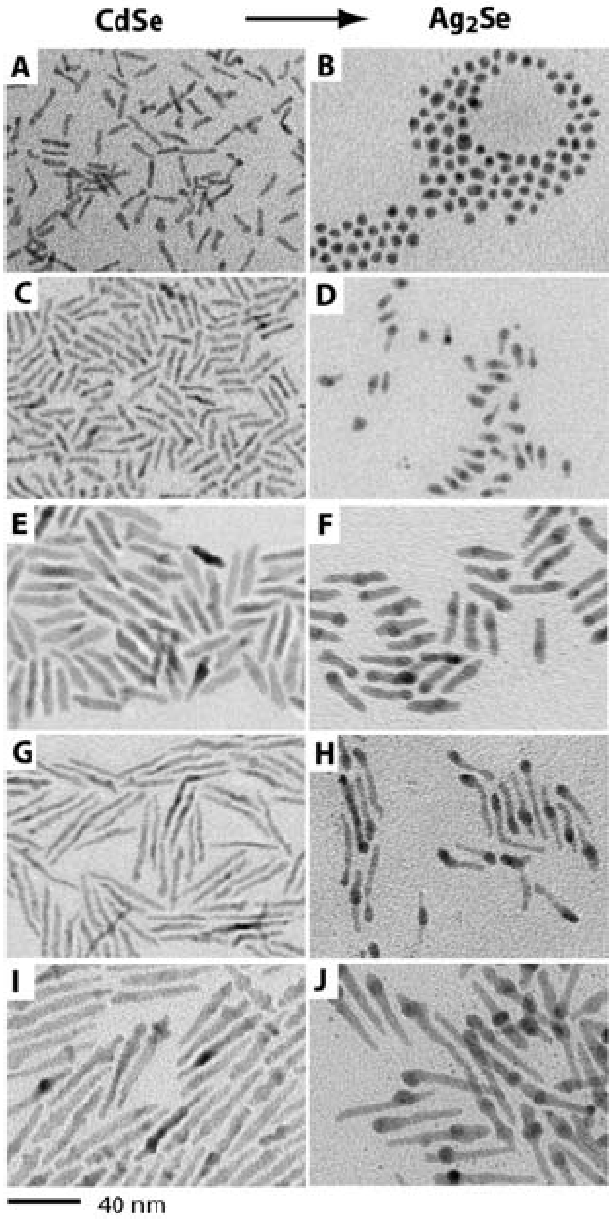

Figure 1.3: TEM images of CdSe nanorods of different sizes (A, C, E, G, and I) and their transformed Ag_2Se crystals (B, D, F, H, and J). As the nanorods become thicker from (A) to (I), the shape change during the cation exchange reaction is suppressed.[29]

Besides the result reported by Alivisatos, Moon and co-workers succeeded in synthesizing various ultrathin metal telluride nanowires of M_xTe_y (M = Ag, Cd, Zn, Pb, and Pt).[30] The Ag_2Te nanowires were converted into CdTe, ZnTe, and PbTe using cation-exchange reactions, and the CdTe nanowires were further transformed into $PtTe_2$ nanotubes. Figure 1.4 shows the TEM images of the transformed metal telluride nanowires. All of the nanowires were found to preserve the initial morphology of the Ag_2Te nanowires. The crystal lattices of the nanowires obtained from HRTEM micrographs can be indexed as zinc blende for CdTe, ZnTe, and NaCl-type cubic structure for PbTe nanowires.

The governing factors for proper transformations should be considered as the follows: (1) the thermodynamic parameters that determine the transformation direction (forward and backward), (2) the kinetics of a transformation (activation barrier), (3) the effect of mechanical stress on retaining the initial shape, and (4) the mechanisms of transformations (the way of diffusion for foreign cations). When an ionic solid crystal has lower solubility than a reactant in the reaction medium, a forward reaction of ion exchange may occur. If the condition is satisfied, the kinetics can be controlled by adjusting reaction temperature to overcome the activation energy.

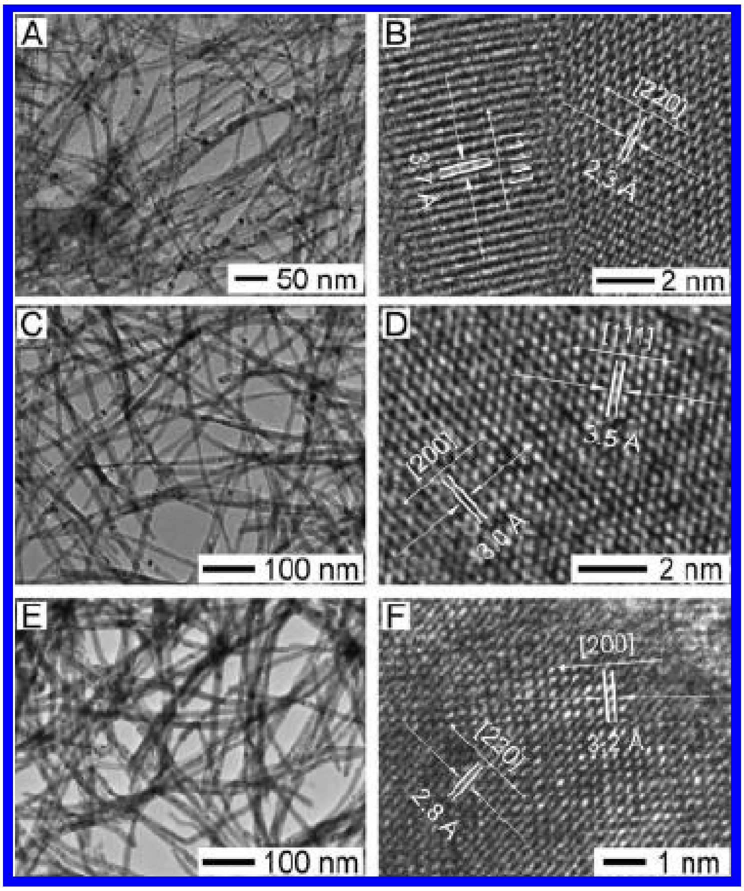

Figure 1.4: TEM and HRTEM images of (A,B) CdTe, (C,D) ZnTe, and (E,F) PbTe nanowires derived from Ag_2Te nanowires. [30]

The chemical transformations in our study are illustrated in Scheme 1. The as-synthesized Se nanorods were first prepared and then transformed into Ag_2Se nanorods. After that, the Ag_2Se nanorods were converted into CdSe, ZnSe, and $Cd_{1-x}Zn_xSe$ alloyed nanorods via cation exchange approach. We showed that cation exchange reactions can occur completely in ionic nanocrystals at ambient pressure.

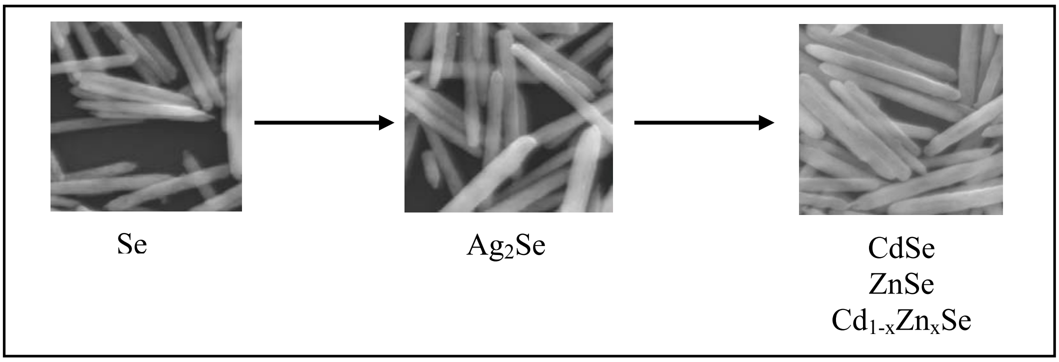

Scheme 1: Summary of the transformations investigated in this study. The as-synthesized Se nanorods were transformed into Ag_2Se nanorods by direct incorporation of Ag^+ into Se nanorods. After that, the Ag_2Se nanorods were converted into CdSe, ZnSe, and $Cd_{1-x}Zn_xSe$ alloyed nanorods through cation exchange reactions.

II. METHOD AND ANALYSIS

1. Chemicals

All chemicals were used without further purification.

1. Selenium (IV) oxide (SeO_2), 98%, Aldrich

2. Sodium borohydride ($NaBH_4$), 96%, Fluka

3. Sodium hydroxide (NaOH), 98%, Mallinckrodt

4. Carboxymethyl cellulose (CMC), Sodium salt, 98%, Sigma

5. Silver nitrate ($AgNO_3$), 99.9%, J.T.Baker

6. Zinc nitrate tetrahydrate ($N_2O_6.4H_2O$), 98%, Riedel-deHaën

7. Cadmium nitrate hexahydrate ($CdN_2O_6.6H_2O$), 98%, Fluka

8. Tri-Butyl Phosphate (TBP), 96%, Kanko Chemical

9. Polyvinylpyrrolidone (PVP), M.W. = 10000, 99%, Sigma Aldrich

10. Absolute Methanol (CH_3OH), Mallinckrodt

2. Instruments and Principles

1. X-Ray Diffractometer (XRD): MAC Science, MXP18, operated at 40kV and 30mA

2. Field-Emission Scanning Electron Microscope (FESEM): JEOL, JSM-6500F, operated at 15 kV

3. Transmission Electron Microscope (TEM): Philips Tecnai, F20G2, operated at 200kV

4. UV-Visible Spectrophotometer: Hitachi, U-3900H

2.1. X-Ray Diffractometer

In XRD, a constructive interference is produced through the interaction of the incident X-ray with the sample under the regime of Bragg's Law ($n\lambda = 2d \sin \theta$). This law correlates the wavelength of X-ray (λ) with the diffraction angle (2θ) and the lattice spacing of crystal (d) of the sample. By scanning the sample through a wide 2θ range to collect primary diffraction peaks, one may identify the crystal structure of sample by referring to the standard reference patterns.

2.2. Scanning Electron Microscope (SEM)

The kinetic energy of accelerated electrons in SEM is dissipated as many different signals when hitting the sample surfaces. These signals mainly include secondary and backscattered electrons. Secondary and backscattered electrons are then collected and used for imaging the morphology and compositional contrast of samples, respectively.

2.3. Transmission Electron Microscope (TEM)

In TEM, the electrons are focused with electromagnetic lenses and transmitted through the sample to image and analyze the microstructure. The electron beams are basically accelerated at several hundred kV, producing wavelength much smaller than that of light. For example, 200 kV of acceleration voltage produces electron beam with a wavelength of 0.025Å. The resolution of TEM is however limited by aberrations inherent in electromagnetic lenses, which is about 1-2 Å.

2.4. Ultraviolet–visible Spectroscopy

Absorption of incident radiation by the electrons in materials usually leads to a high frequency, i.e. low wavelength, absorption band that can be observed in the range of 200 to 800 nm. For a solution containing an absorbing substance, the absorptivity ratio at a fixed wavelength is defined as Io/I, which is logarithmically related to the concentration of solute (c) and the optical path length of sample cell (b) according to the Beer Lambert law: Absorbance (A) = $\log_{10}(Io/I) = \alpha\, b\, c$, where α is a constant named absorption coefficient.

3. Preparation of Se and Ag_2Se Nanorods

3.1. Preparation of Se Nanorods:

Following a procedure developed by our group, firstly, 0.082g of SeO_2 (0.74 mmole) was dissolved in 9ml of CMC solution (4.0wt%), 1ml of NaOH solution (C_M = 1M) was then added with vigorous stirring at room temperature in water-bath until the solution turned to transparent. After that, 0.03g (0.79 mmole) of $NaBH_4$ dissolved in 1ml deionized water was added into the above solution with the rate of 100μl/sec. The mixed solution color changed quickly from transparent to brick red, then to brown after 4 hours stirring at room temperature. This brown solution was then centrifuged at 8000 rpm for 20 min and washed with deionized water and ethanol to remove remaining ions and impurities. The washed powder (Se nanorods) was finally dried at 60^{o}C in vacuum for 6 hours.

3.2. Preparation of Ag_2Se Nanorods:

The procedure also followed the one done by our group. First of all, 0.0395g of Se (0.5 mmole) nanorods were re-dispersed in 10ml of deionized water (A solution). After that, 1.25 mmol of $AgNO_3$ dissolved in 10 ml water was added into A gradually. The mixed solution was then stirred vigorously at room temperature. When the color of solution turned to black after 5 hours, the experiment was stopped. The product (Ag_2Se nanorods) was collected by centrifugation at 8000 rpm for 10 min and washing with distilled water and ethanol for several times, then drying at 60°C in vacuum for 6 hours.

4. Preparation of CdSe, ZnSe and $Cd_{1-x}Zn_xSe$ Alloyed Nanorods

CdSe, and ZnSe and alloyed $Cd_{1-x}Zn_xSe$ nanorods were produced by using the cation exchange approach from the as-synthesized Ag_2Se nanorods. 0.0147g of Ag_2Se nanorods (0.5×10^{-4} mole) were re-dispersed in 10ml of methanol and put into a three-neck round bottom flask (solution A). $Cd(NO_3)_2$ and $Zn(NO_3)_2$ was then dissolved in 40ml of methanol contained 0.5g of PVP (solution B). The molar ratios of Cd^{2+}/Zn^{2+} used in this work are 1:0, 1:1, 1:2, 1:4, 0:1. After that, the solution B was added into the solution A at the temperature of 65°C. 500μl of TBP solution was injected into the above mixed solution to proceed with the cation exchange reaction. The experiments were carried out using reflux system to make sure that the volume of the mixture solution would not change during the reaction. After the reaction time of 20 hours under vigorously stirring condition, Ag_2Se was converted into CdSe (ZnSe or $Cd_{1-x}Zn_xSe$ alloys) completely. The final products (CdSe, ZnSe, and alloyed $Cd_{1-x}Zn_xSe$) were collected by centrifugation at 8000 rpm for 5 minutes and washed with distilled water and methanol for several times.

Scheme 2 illustrates the procedures to synthesize Se, Ag_2Se, CdSe, ZnSe and alloyed $Cd_{1-x}Zn_xSe$ nanorods as describes above.

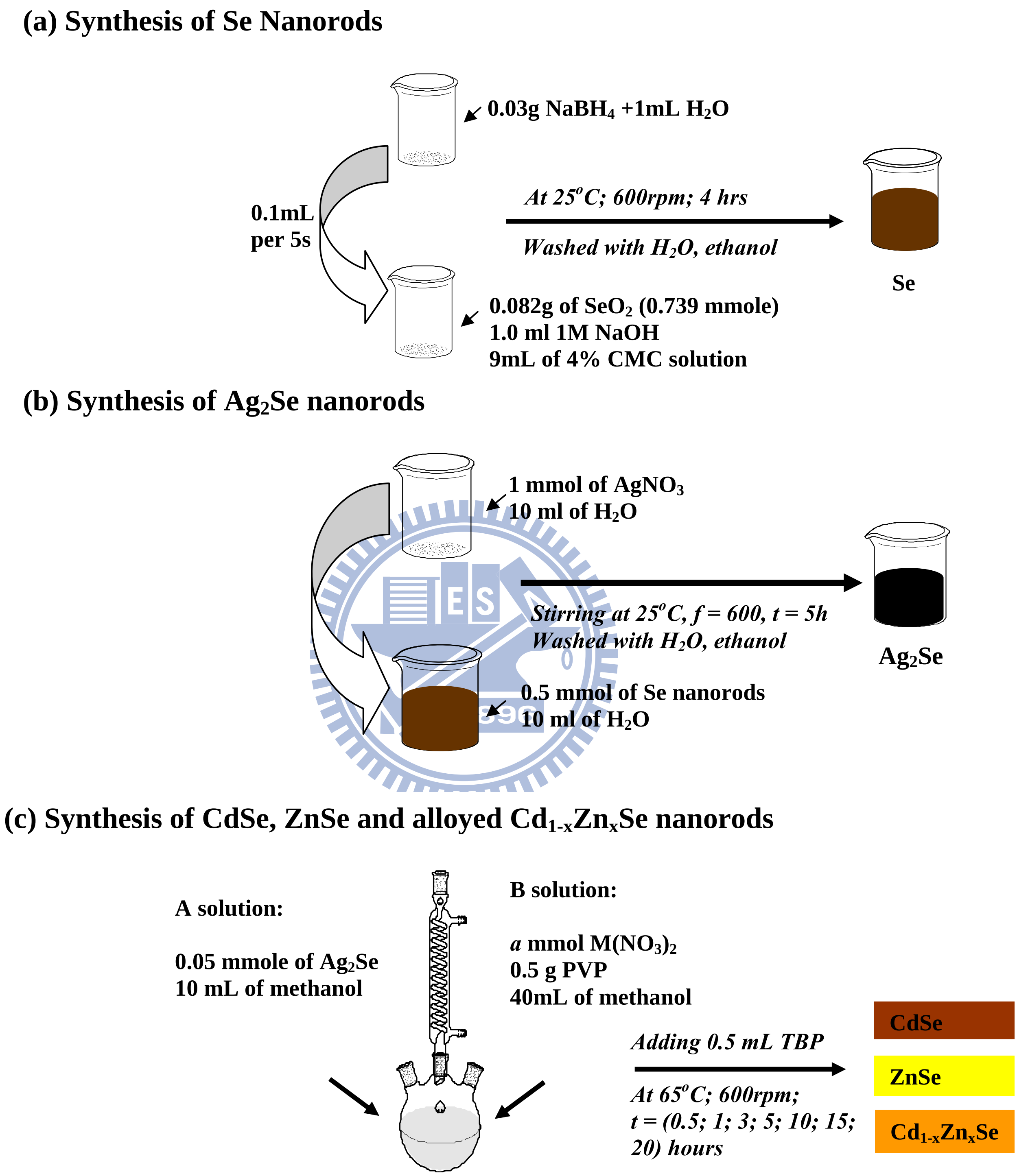

Scheme 2: Illustration of the procedures to synthesize (a) Se nanorods; (b) Ag_2Se nanorods; (c) CdSe, ZnSe and $Cd_{1-x}Zn_xSe$ alloyed nanorods.

5. **Photocurrent Measurement**:

A mercury-xenon lamp was used as a light source. The light intensity was calibrated with a power meter (Rapitech Enterprise Co., Ltd), but no correction was made for the reflections. The electrochemical cell was under a flowing nitrogen atmosphere (but without bubbling) to eliminate the influence of oxygen. Before measurement, the electrolyte solution was bubbled with N_2 for 10 min. Photocurrent measurement were carried out in a three-armed cell with a Pt-gauze counter electrode and an Ag/AgCl electrode as a reference. An aqueous 0.1 M Na_2S solution was used as an electrolyte in all of the measurement reported here. FTO substrates that contained various nanorods were used as working electrodes. Prior to the deposition of nanorods, the FTO-coated glass (10×10 mm^2) was cleaned with ethanol for 15 min sequentially in an ultrasonic bath. The working electrode was prepared by dropping 10 μL of 5mg/mL of nanorod solution onto FTO-coated glass substrate, respectively. All measurements were carried out under ambient conditions.

6. Characterization

The morphology of the products was examined by a FESEM (Jeol, JSM-6500F) and a TEM. The crystallographic structure of the samples was investigated with XRD (MAC Science, MXP18) and HRTEM (Philips Tecnai, F20 G2) operated at 200kV. The composition of the products was obtained by the energy dispersive X-ray (EDX) Spectrometer from FESEM and TEM. The photocurrent measurement of nanorods was carried out using photoelectrochemical approach as described above. UV-visible absorption spectra were recorded using a Hitachi U-3900H at room temperature under ambient atmosphere.

III. RESULTS AND DICUSSION

1. Synthesis of Se and Ag_2Se Nanorods

Se Nanorods: The FESEM image from Figure 3.1a shows the morphology of Se nanorods prepared from the reduction of SeO_2 by $NaBH_4$ in the presence of CMC. The dimension of the as-prepared Se nanorods was about 50-70 nm in diameter and 500-800 nm in length. The compositional information of nanorods was then studied by XRD. The corresponding XRD pattern as shown in Figure 3.1c confirms the formation of elemental Se. All the diffraction peaks in this spectrum can be indexed as the hexagonal phase of Se by referring to the reference (JCPDS, NO. 65-3404). SEM and XRD results confirm the success in synthesizing Se nanorods with considerably uniform dimensions.

Direct Introduction of Ag+ into Se Nanorods: It should be pointed out that Ag_2Se can be formed through a direct introduction of Ag^+ onto Se crystals at room temperature. The reaction in this process can be shown as follows:

$$3Se_{(s)} + 6Ag^+_{(aq)} + 3H_2O \rightarrow 2Ag_2Se_{(s)} + Ag_2SeO_{3\,(aq)} + 6H^+$$ [40]

A molar ratio of 2:1 of Ag^+ to Se nanorods produced pure Ag_2Se nanocrystals. The EDX analysis from Figure 3.1e displays that the chemical component of the sample consists of Ag and Se. The corresponding atomic percentages of Ag and Se are 34.46% and 16.54%, respectively. In addition, all the XRD peaks taken from Ag_2Se sample are in good agreement with the corresponding reference data of orthorhombic Ag_2Se, with the lattice constants being a = 4.33 A^{o}, b = 7.06 A^{o}, and c = 7.76 A^{o} (JCPDS 24-1041).

On the other hand, the SEM and TEM results in Figures 3.1b, d, f confirmed that Ag_2Se nanocrystals derived from Se nanorods had rod-like morphology. The diameter and length of Ag_2Se nanorods remained unchanged compared to those from Se nanorods.

\

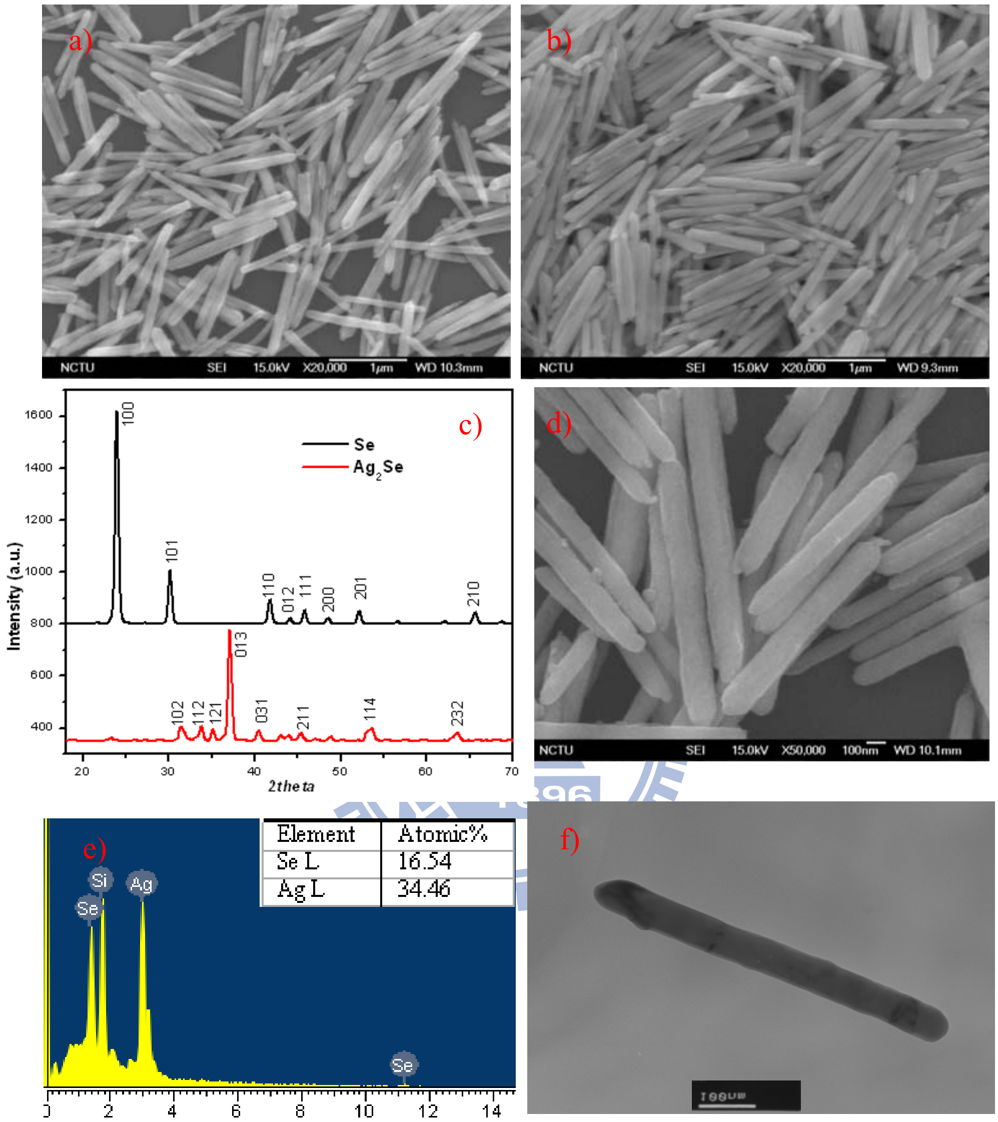

Figure 3.1: a) FESEM image of Se nanorods; b), d) Typical FESEM and a high-magnification FESEM image of Ag_2Se nanorods derived from Se nanorods, respectively; c) XRD patterns of Se and Ag_2Se nanorods; e) SEM-EDX result for Ag_2Se nanorods; f) TEM image of a single Ag_2Se nanorod.

2. Transformation of Ag_2Se Nanorods into CdSe, ZnSe and $Cd_{1-x}Zn_xSe$ alloyed Nanorods via Cation Exchange Reactions.

2.1. Morphology of $Cd_{1-x}Zn_xSe$ Nanocrystals

After placing Ag_2Se into the solvent, the reaction could be carried out in three ways: (1) Simultaneous injection of both precursors; (2) injection of cadmium precursor followed by injection of zinc precursor; (3) injection in the reverse order. By using method (1) in our experiment, we showed that the morphology of the reaction products can be preserved as that of the initial sample. The prototypical semiconductor nanocrystal system of Ag_2Se reacts with Cd^{2+}, Zn^{2+} ions to yield CdSe, and ZnSe and alloyed $Cd_{1-x}Zn_xSe$ nanocrystals by the cation exchange reaction. Figure 3.2 shows the SEM images of a series of $Cd_{1-x}Zn_xSe$ nanorods obtained with varying amounts of zinc and cadmium precursors, as indicated in Table 3.1. This table also contains the composition of final products determined by EDX analysis. It is very clear that the morphology of these alloyed nanorods is similar to that of initial Ag_2Se. The nanorods have diameters of 50-70 nm and lengths can be varied from 500 to 800 nm. Furthermore, we observed in all experiments that the composition of the $Cd_{1-x}Zn_xSe$ nanorods is mainly dependent on the amount of Zn^{2+} and Cd^{2+} precursors used and the intrinsic Zn^{2+} and Cd^{2+} reactivity. It is worth mentioning that the Zn^{2+} precursor has lower reactivity, compared to Cd^{2+} precursor (as inferred in Table 3.1).

Table 3.1: Experimental conditions in the synthesis of $Cd_{1-x}Zn_xSe$ nanorods

Sample No.	Composition (x in $Cd_{1-x}Zn_xSe$)	Cadmium nitrate [mmol]	Zinc nitrate [mmol]
1	0	2	0
2	0.35	1	1
3	0.54	0.7	1.4
4	0.61	0.4	1.6
5	1	0	2

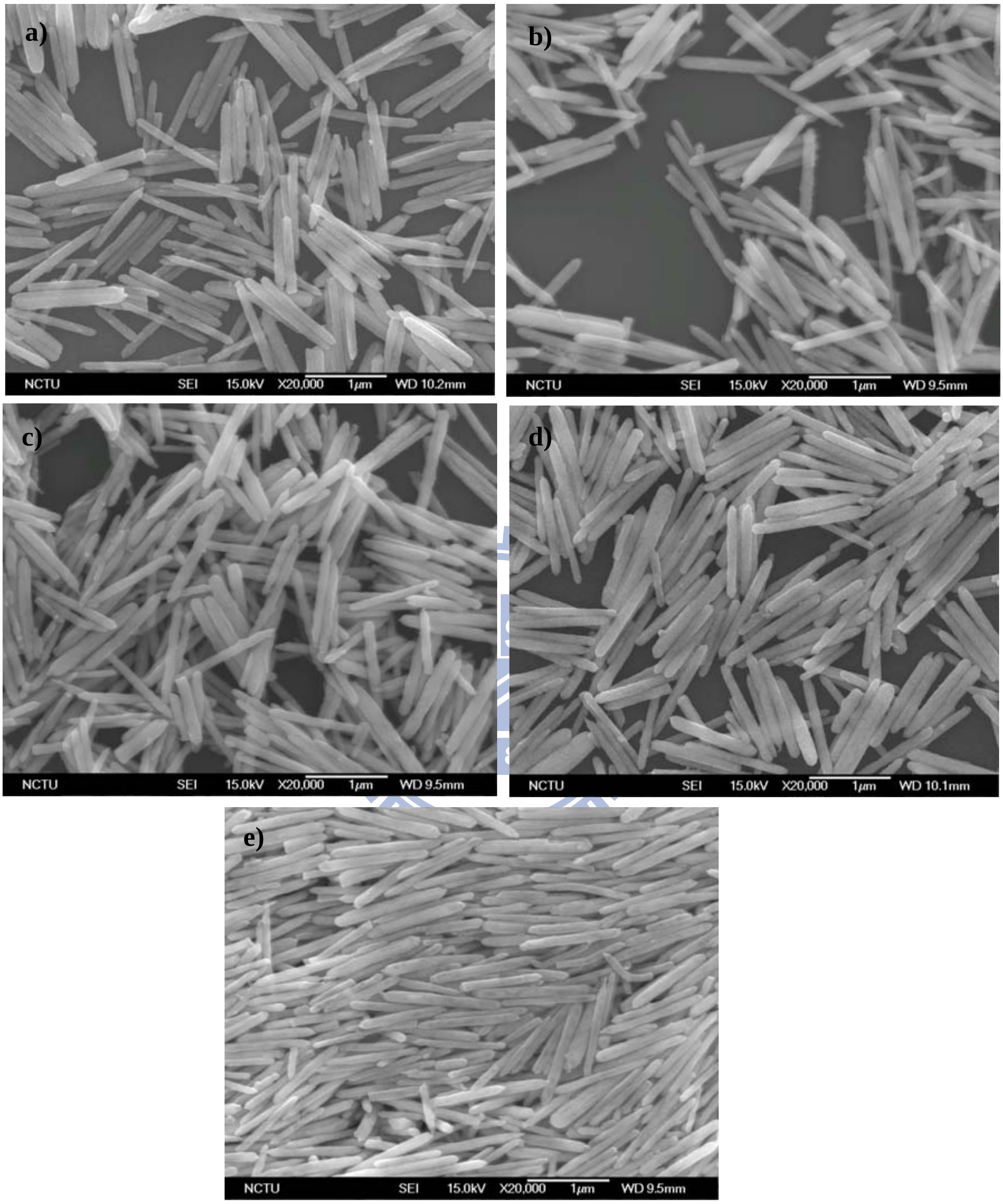

Figure 3.2: FESEM images of a) CdSe, b) $Cd_{0.65}Zn_{0.35}Se$, c) $Cd_{0.46}Zn_{0.54}Se$, d) $Cd_{0.39}Zn_{0.61}Se$, e) ZnSe nanorods. The CdSe, ZnSe and alloyed $Cd_{1-x}Zn_xSe$ nanorods were derived from Ag_2Se nanorods via cation exchange process. The morphology of nanorods remained unchanged after the reactions.

To obtain more details about structures of $Cd_{1-x}Zn_xSe$ nanorods, HRTEM and SAED measurements were exploited. Figures 3.3 and 3.4 show the TEM images of the CdSe, ZnSe and $Cd_{0.65}Zn_{0.35}Se$ nanorods. All of the nanorods turned out to preserve the initial morphology of the Ag_2Se nanorods. The crystal lattices of the nanorods obtained from HRTEM micrographs can be indexed as wurtzite structure for both CdSe and ZnSe nanorods. HRTEM images in Figure 3.3d shows that ZnSe nanorods have interplanar spacing of 0.19 nm, which corresponds to the separation between (110) of the hexagonal crystal structure. The interplanar spacing of CdSe nanorods is 0.22 nm, indicating the separation between (110) (see Figure 3.3d). For the alloyed nanorods of $Cd_{0.65}Zn_{0.35}Se$, the interplanar spacing was observed as 0.21 nm, also indicating the separation between (110), as shown in Figure 3.4c.

The HRTEM images in Figures 3.3d, 3.3e and 3.4c show a growth direction of [110] observed for CdSe, ZnSe and alloyed $Cd_{0.65}Zn_{0.35}Se$ nanorods. In addition, the dot-pattern of SAED (see the insets of Figures 3.3d, 3.3e and 3.4c) reveals the poly-crystallinity of ZnSe nanorods and single-crystallinity of both CdSe and alloyed $Cd_{0.65}Zn_{0.35}Se$ nanorods, respectively.

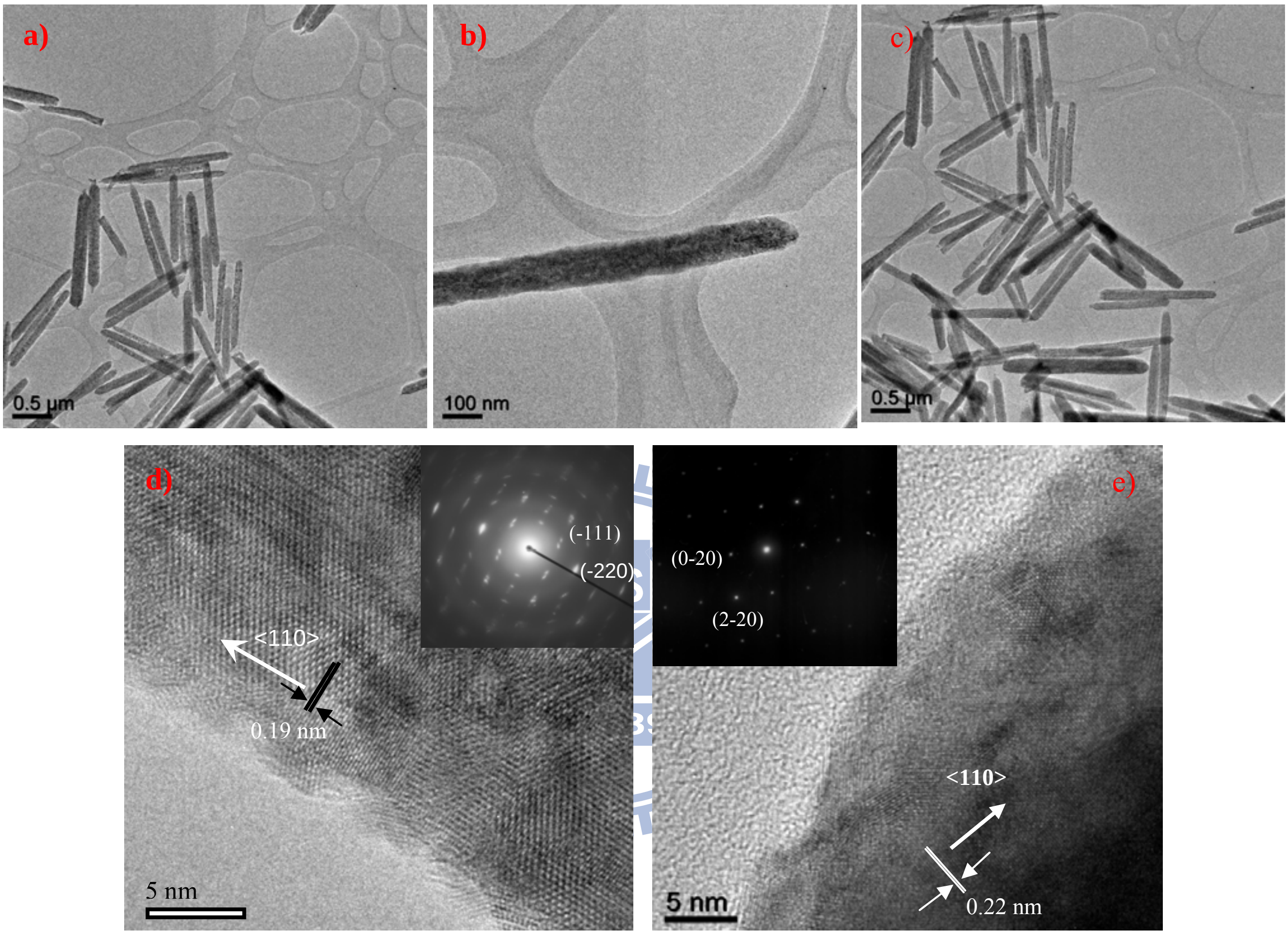

Figure 3.3: a) and b) TEM images at different magnifications of ZnSe nanorods, c) TEM image of CdSe nanorods, d) and e) HRTEM images and electron diffraction pattern (see the inset) of ZnSe and CdSe nanorods, respectively.

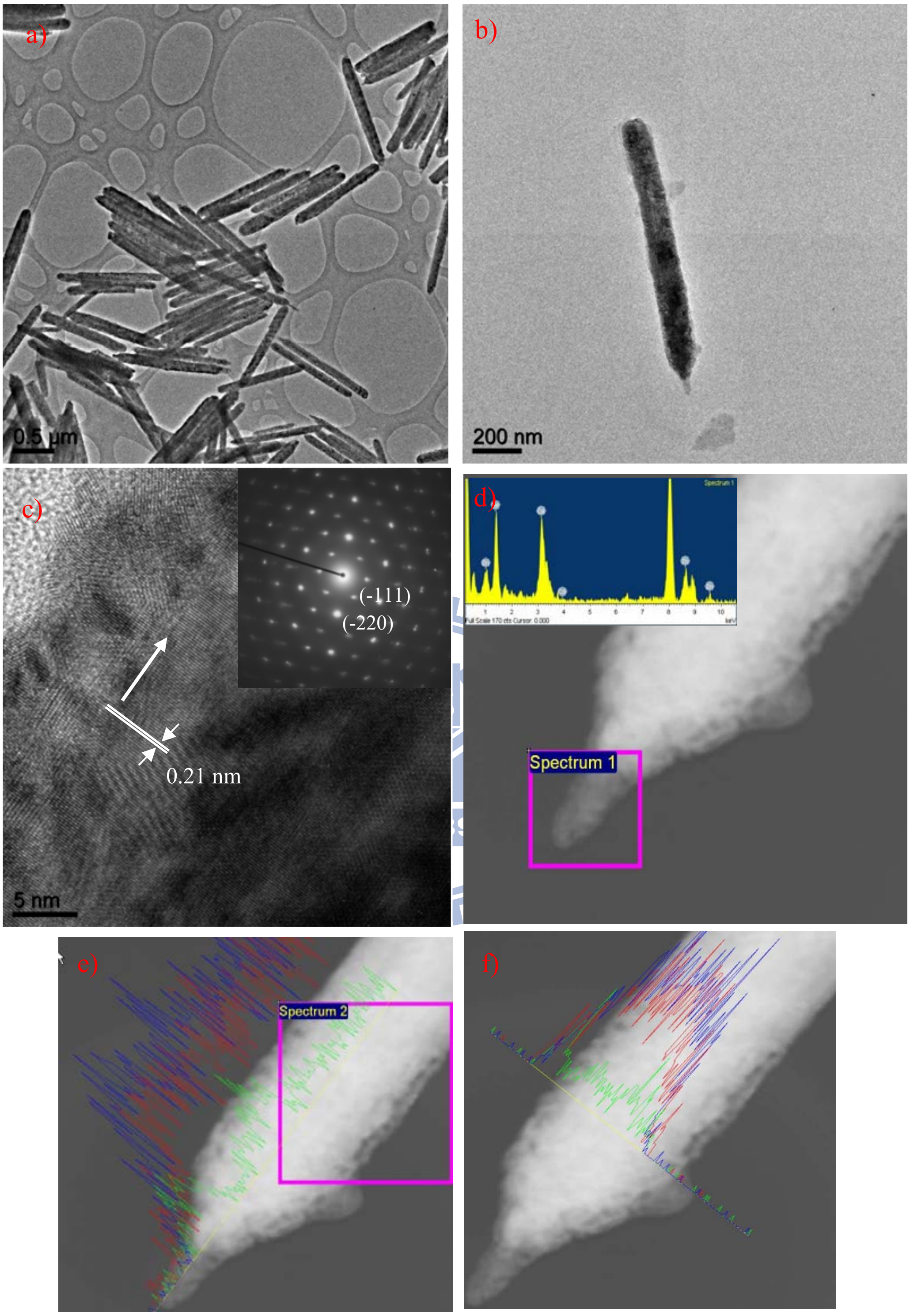

Figure 3.4: a) and b) TEM images at different magnifications, c) HRTEM image and electron diffraction pattern (see the inset), d) EDX spectrum, e) and f) Line-scan EDX profiles of $Cd_{0.65}Zn_{0.35}Se$ alloyed nanorods for cadmium (red signal), zinc (green signal), selenium (blue signal).

2.2. Crystallographic Structures of $Cd_{1-x}Zn_xSe$ Nanorods

The XRD patterns of the $Cd_{1-x}Zn_xSe$ nanorods (x = 0, 0.35, 0.54, 0.61) shown in Figure 3.5 indicate a complete cation exchange between Ag^+ and Cd^{2+} and Zn^{2+}. In addition, the three alloyed nanorods all exhibited the hexagonal crystal structures. The peak positions of three alloyed nanorods are in between the ones of the corresponding peaks of CdSe and ZnSe. As the composition of Zn increases, the diffraction peaks gradually shift toward higher 2θ regions, which is indicative of the transformation from the CdSe to the ZnSe lattice.

The CdSe nanorods were crystallized in the wurtzite structure with a = 4.31 A^o, c = 7.02 A^o (JCPDS 65-3415). For ZnSe case, the XRD pattern can also be indexed to the hexagonal phase (wurtzite structure). The lattice constants are a = 3.99 A^o, c = 6.27 A^o (JCPDS 89-2940).

A gradual increase in lattice spacing along the axial direction is observed with the decrease of Zn content in the nanorods (1.9 A^o for ZnSe, 2.1 A^o for $Cd_{0.65}Zn_{0.35}Se$, and 2.2 A^o for CdSe, as determined from HRTEM). This trend confirms the formation of alloys with homogeneous distribution of ZnSe inside the CdSe matrix.

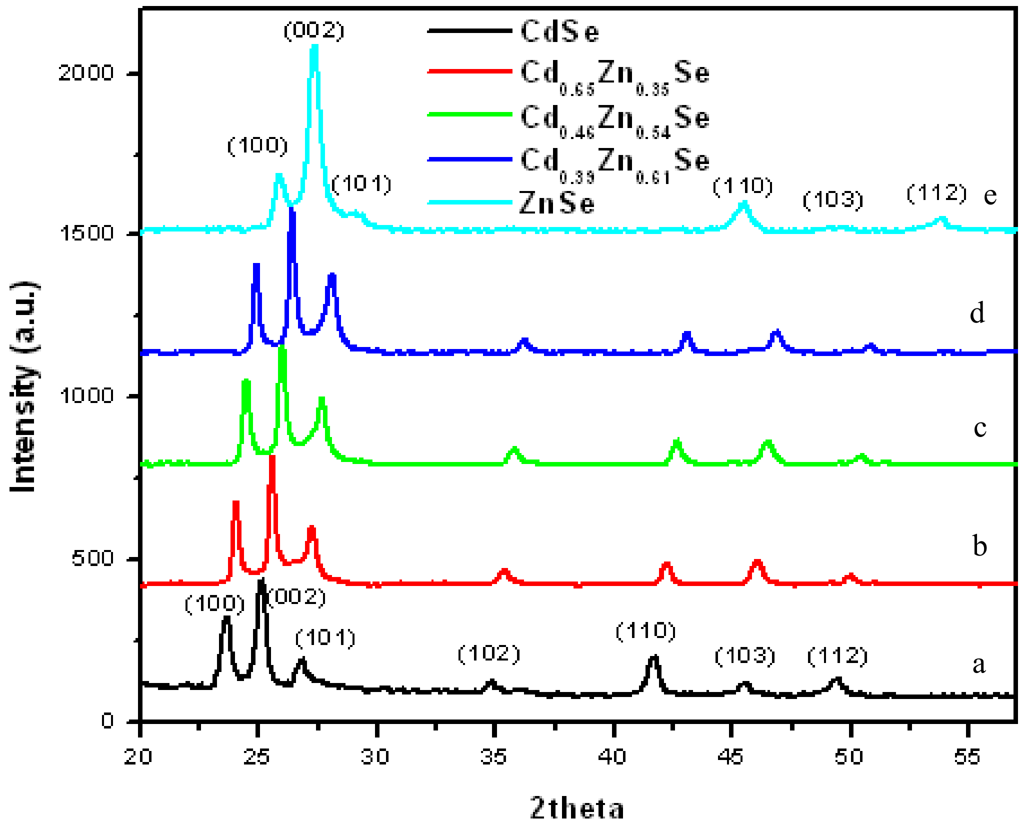

Figure 3.5: XRD patterns of $Cd_xZn_{1-x}Se$ nanorods with different Zn mole fractions of a) 0, b) 0.35, c) 0.54, d) 0.61 and e) 1. The peaks shift toward the higher angle with the increase of zinc molar ratio from 0 to 1.

The chemical transformations were also characterized using SEM-EDX, as shown in Figure 3.6. The EDX results indicate a complete replacement of Ag^+ by Cd^{2+} and Zn^{2+} ions in the cation exchange reactions. All peaks indexed to Ag in Ag_2Se nanorods disappeared after the cation exchange reaction, while peaks assigned to Zn or Cd. The atomic percentages obtained from EDX data for CdSe were Cd = 17.3% and Se = 17.4%. For ZnSe, the atomic percentages of Zn and Se were 9.11% and 8.98%, respectively. The atomic ratios of Cd (or Zn) and Se are almost 1:1. These results are in good accordance with the XRD analyses mentioned above.

Besides, Figures 3.6 b, c, and d show the atomic percentages of Cd, Zn and Se of the three $Cd_{1-x}Zn_xSe$ alloyed nanorods. Determination of Cd:Zn ratio yields x = 0.35, 0. 54, 0.61 with the increase of initial zinc molar ratio as shown in Table 3.1.

Furthermore, the TEM-EDX analyses shown in Figures 3.4e and 3.4f are evidences to prove that the $Cd_{0.65}Zn_{0.35}Se$ nanorods are alloyed, neither core-shell structure nor the separation of CdSe and ZnSe nanocrystals. Zinc composition distributes randomly on the rod.

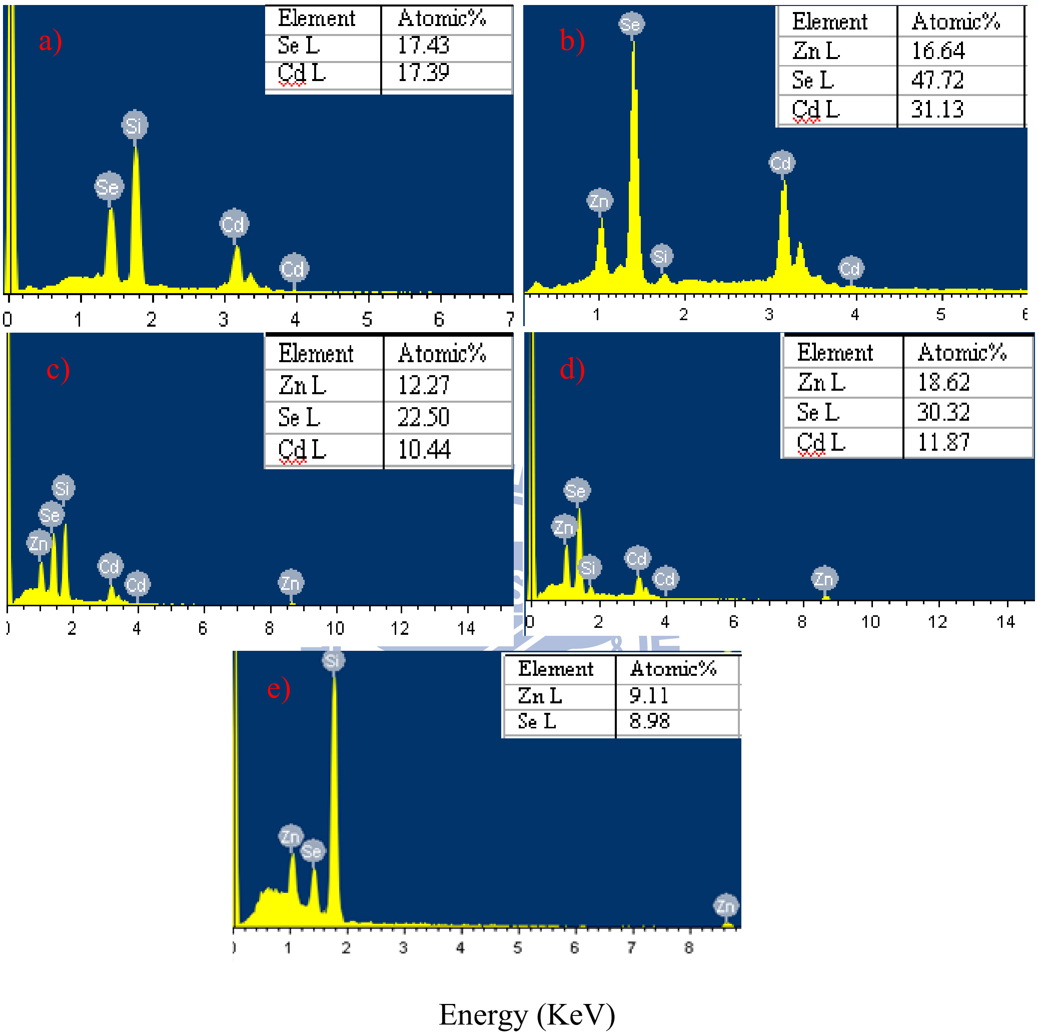

Figure 3.6: EDX spectra taken from a) CdSe, b) $Cd_{0.65}Zn_{0.35}Se$, c) $Cd_{0.46}Zn_{0.54}Se$, d) $Cd_{0.39}Zn_{0.61}Se$, e) ZnSe nanorods.

3. The Growth Mechanism of CdSe, ZnSe and $Cd_{1-x}Zn_xSe$ Nanorods

In order to perform the cation exchange reactions, the Ag_2Se nanorods were redispersed in methanol, and PVP was added as a stabilizer to prevent any possible agglomeration during the cation exchange process. We used nitrate salts as the precursors because they are highly soluble in methanol, the solvent used for all cation exchange reactions.

In our research, TBP also played an important role because no cation exchange was observed without TBP. TBP is believed to be able to bind to both Ag^{+} ions in the nanorods and Cd^{2+} (or Zn^{2+}) ions in solution, forming intermediate complexes. Methanol may act as a ligand, together with TBP, to form intermediate complexes.[30]

In our experiment, the reaction took place right after the injection of TBP. The color of the resulting solutions was brown for CdSe, yellow for ZnSe, and brownish yellow for alloyed samples (see Figure 3.7). Furthermore, the morphology of $Cd_{1-x}Zn_xSe$ nanorods kept unchanged during the cation exchange reaction. This is confirmed by FESEM images of CdSe and ZnSe nanocrystals with different reaction times, as indicated in Figure 3.9 and Figure 3.10, respectively.

As mentioned above, the Zn^{2+} precursor has lower reactivity than Cd^{2+} precursor. This is also inferred from the change in Ag:Cd molar ratio (in synthesis of CdSe), Ag:“Cd+Zn” molar ratio (in preparation of three alloyed nanocrystals), and Ag:Zn molar ratio (for ZnSe case) when the reaction time increased from 0 to 20 hours (see Figure 3.8 and Table 3.2). In the synthesis of $Cd_{1-x}Zn_xSe$ nanorods, the reaction rate increases with the increase of cadmium molar ratio. Besides, the reaction rate in preparation of CdSe is higher than that of ZnSe and three alloyed nanocrystals.

Figure 3.7: Photograph of water suspensions of Se, Ag_2Se, and $Cd_{1-x}Zn_xSe$ nanorods obtained in this study.

Table 3.2: The variation in molar ratios of Ag/M (M = Cd; Zn; “Cd+Zn”) for nanorods with the increase of the reaction times.

Molar ratio / Reaction times	Ag/Cd (CdSe)	Ag/”Cd+Zn” ($Cd_{0.65}Zn_{0.35}Se$)	Ag/”Cd+Zn” ($Cd_{0.46}Zn_{0.54}Se$)	Ag/”Cd+Zn” ($Cd_{0.39}Zn_{0.61}Se$)	Ag/Zn (ZnSe)
0.5	1.87	7.37	5.89	7.7	5.15
1	0.97	2.09	2.37	4.35	4.29
3	0.19	0.16	0.27	1.18	1.98
5	0.09	0.12	0.12	0.21	0.94
10	0.06	0.09	0.09	0.14	0.16
20	0	0	0	0	0

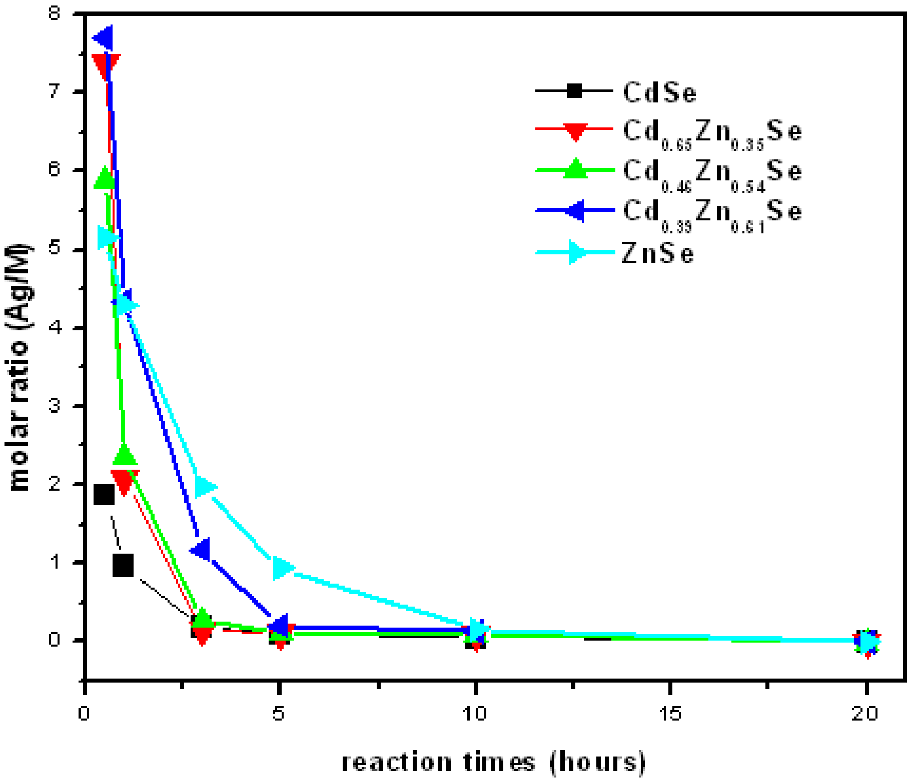

Figure 3.8: Plots of the change in molar ratios of Ag/Cd, Ag/“Cd +Zn”, Ag/Zn for nanorods with the increase of reaction times.

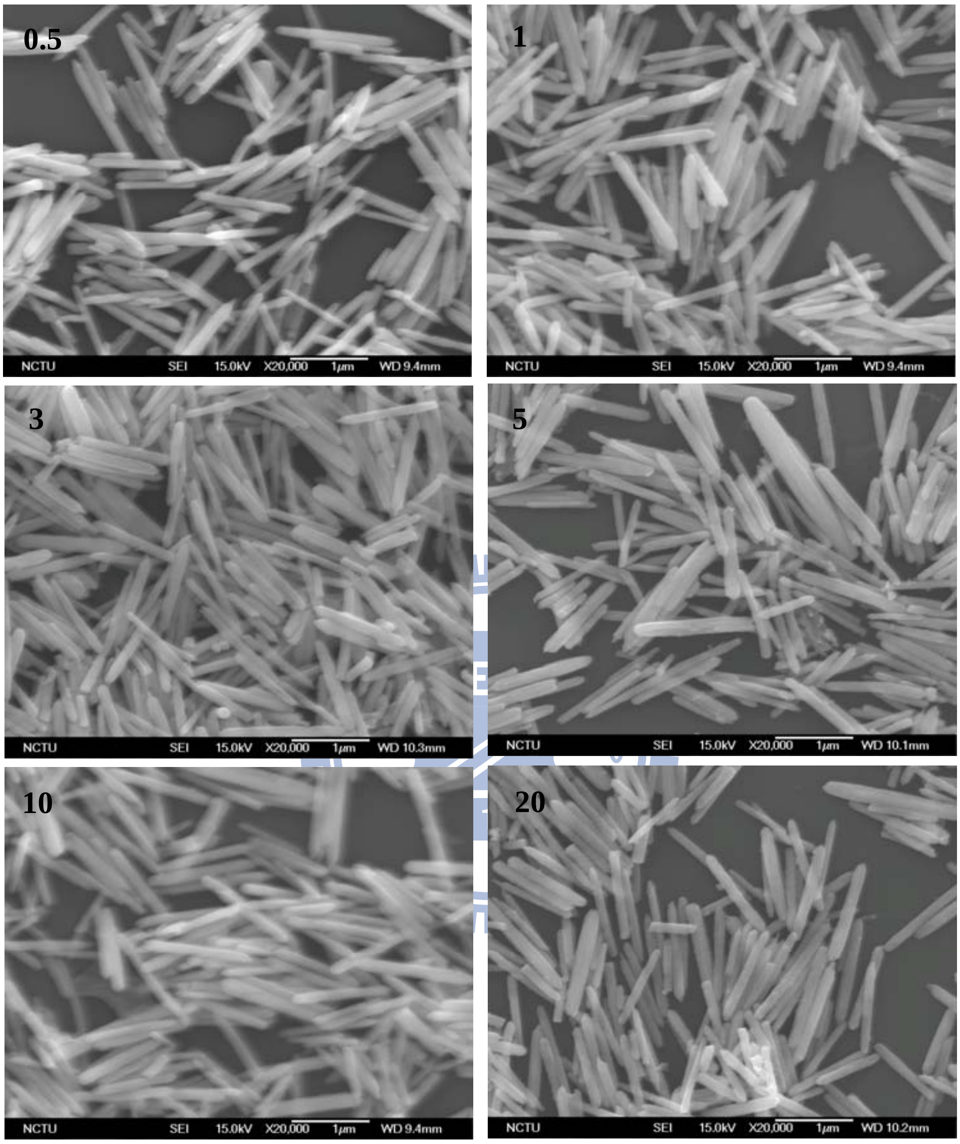

Figure 3.9: FESEM images of CdSe nanorods obtained by cation exchange reaction with different reaction times from 0.5 hr to 20 hrs. Ag^{+} was completely replaced by Cd^{2+} precursors after long reaction time (about 20 hours). The morphology of nanorods remained unchanged.

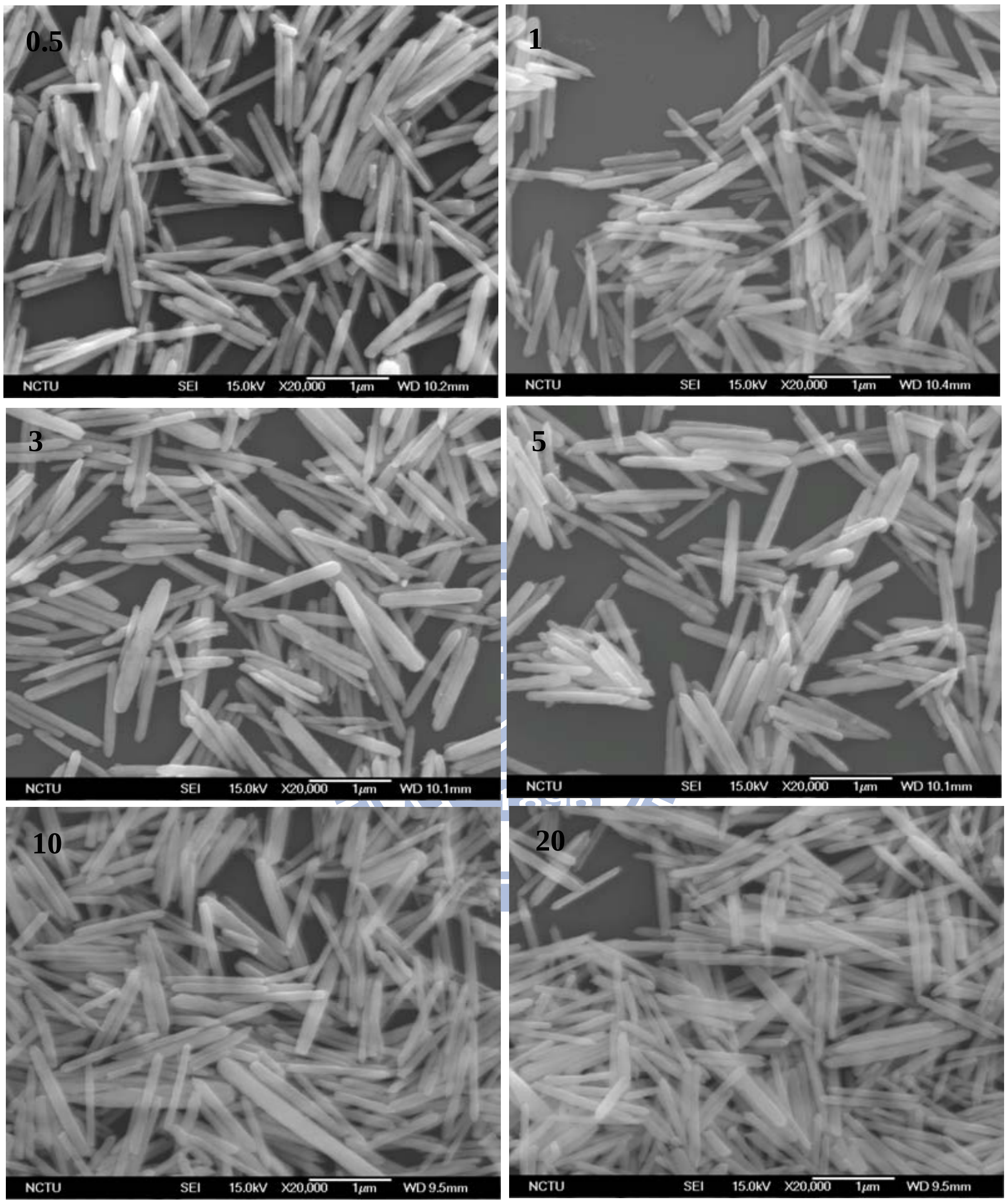

Figure 3.10: FESEM images of ZnSe nanorods obtained by cation exchange reaction with different reaction times from 0.5 hr to 20 hrs. Ag^{+} was completely replaced by Zn^{2+} precursors after long reaction time (about 20 hours). The morphology of nanorods remained unchanged.

It has been reported that the effectiveness in cation exchange between Ag^+ and Cd^{2+} can be explained based on the crystal structures of Ag_2Se and CdSe. The anion sublattice in Ag_2Se (orthorhombic) and CdSe (wurzite) have a topotactic relationship. The *a* and *b* axes of Ag_2Se are almost the same as the *a* and *c* axes of CdSe (a = 4.33 A^o, b = 7.06 A^o in Ag_2Se case, while the lattice constants of CdSe are a = 4.31 A^o, c = 7.02 A^o). This results in matching of anion positions that further facilitates the in and out diffusion of Ag^+ and Cd^{2+} through the lattice, leading to the formation of CdSe without substantial rearrangement for the Se^{2-} sublattice. However, such topotactic relationship between the anion sublattices is not necessarily required in the present nanorod systems, since ZnSe (wurzite) does not show any topotactic relationship with either Ag_2Se or CdSe.

In this context, the stronger interaction between TBP and Ag^+ allows the association of Cd^{2+} with the anion sublattice, leading to the replacement of Ag^+ by Cd^{2+}. The reverse reaction, that is, the replacement of Cd^{2+} by Ag^+, is spontaneous due to the large difference in solubility between Ag_2Se and CdSe ($K_{sp} = 1\times10^{-54}$ mol/L for Ag_2Se and 4×10^{-35} mol/L for CdSe). [30]

Similarly, ZnSe has $Ksp = 1.9 \times 10^{-27}$ which is higher than that of Ag_2Se. On the basis of these numbers, it is expected that the replacement of Ag^+ by

Zn^{2+} will not be spontaneous at room temperature, similar to the replacement of Ag^{+} by Cd^{2+}. Therefore, for the synthesis $Cd_{1-x}Zn_xSe$ nanorods, we had to employ more delicate experimental conditions (i.e., a small amount of TBP together with heating to 65 °C). The difference in solubility between CdSe and ZnSe nanocrystal is another factor that affects the result of cation exchange reaction.

4. Optical Properties of $Cd_{1-x}Zn_xSe$ Nanorods

4.1. UV-vis spectra

The room temperature UV absorption spectra of CdSe, ZnSe and $Cd_{1-x}Zn_xSe$ nanorods in water are shown in Figure 3.11. For semiconductor nanocrystals, the bandgap (E_g) is an important value for electron transportation. Generally, the bandgap of semiconductor nanocrystals could be modulated by controlling the particle size, which has been widely reported. In our research, the optical absorption edge was determined by the optical absorption method [38, 39] and was derived based on the following equation:

$$\alpha h\upsilon = A(h\upsilon - E_g)^{1/2}$$

Where α is the absorption coefficient, Eg is the bandgap, and A is a constant. The variation of $(\alpha h\upsilon)^2$ with photon energy for nanorods is shown and discussed (see inset of Figure 3.11). Bandgap values were obtained by extrapolating the intercepts of the plots (straight lines) on the energy axis. For CdSe and ZnSe nanorods, the bandgap values are 1.75 and 2.58 eV, respectively, which match well with the literature report. The bandgap energy of $Cd_{1-x}Zn_xSe$ nanorods increases from 1.75 to 2.58 eV with the increase in Zn concentration from 0 to 1, as shown in Table 3.3 (E_{g3}).

This general trend is in agreement with that obtained by Kolomiets and Ling [23] who established an empirical second-order function to describe the nonlinear evolution of the bandgap with composition in the bulk alloy.

$$E_{g,bulk}(x) = 1.74 + (0.89 - 0.75)x + 0.75x^2 \qquad (1)$$

On the other hand, in bulk materials, the dependence of E_g on x is also determined by equation 2, where $E^i_{g,\infty}$ is the bulk band gap for i = ZnSe, $Cd_{1-x}Zn_xSe$ or CdSe and b is the bowing parameter (for $Cd_{1-x}Zn_xSe$, b = 0.35). [24]

$$E^{alloy}_{g,\infty} = E^{CdSe}_{g,\infty}(1-x) + E^{ZnSe}_{g,\infty}(x) - bx(1-x) \qquad (2)$$

As anticipated, the bandgap energies (E_g) of the $Cd_{1-x}Zn_xSe$ nanorods in both cases are between those of the CdSe and ZnSe. The bandgap values based on eq. 1 and eq. 2 are E_{g1} and E_{g2} as revealed in Table 3.3, respectively.

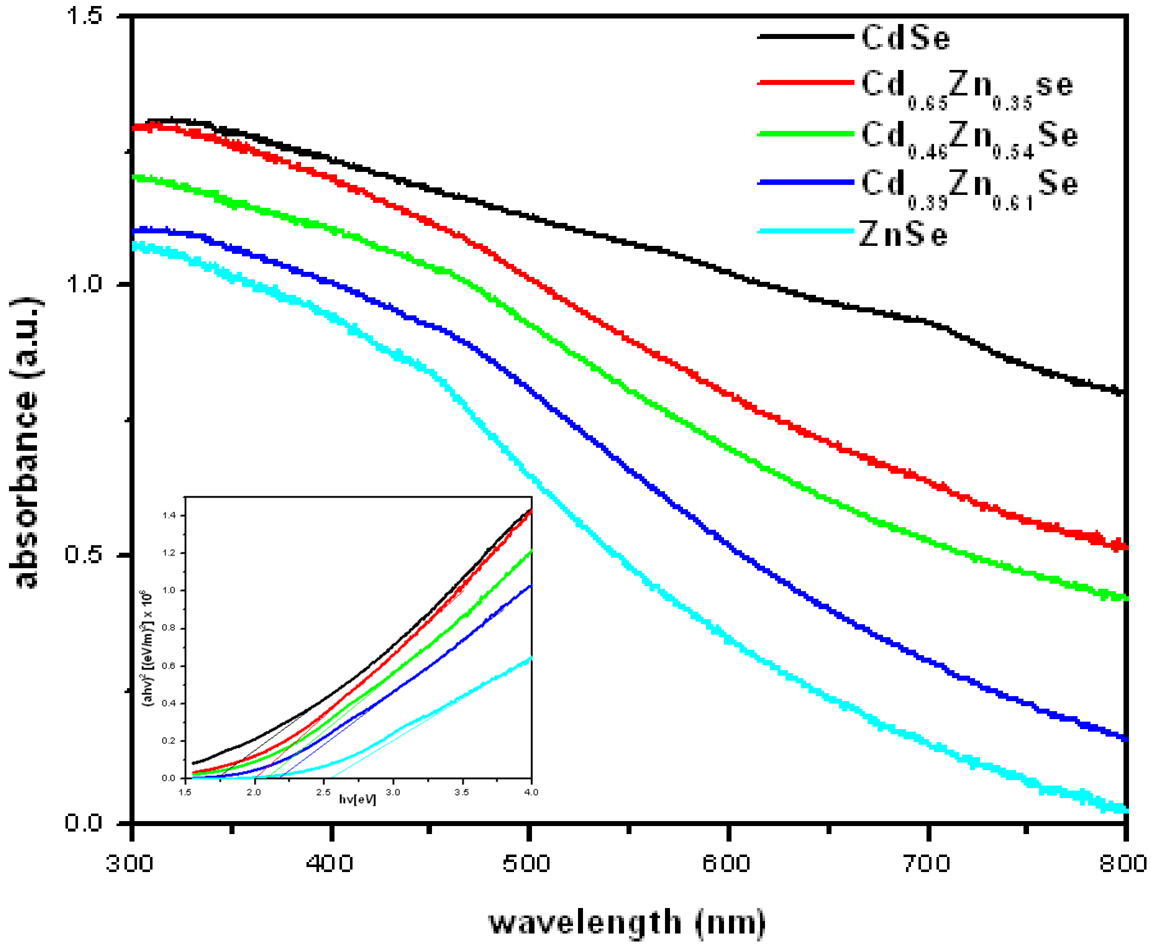

Figure 3.11: Absorption spectra of $Cd_{1-x}Zn_xSe$ nanorods with different Zn/Cd molar ratios. Bandgap values were obtained by extrapolating the linear region in plots of $(\alpha h\upsilon)^2$ vs. photon energy (see inset of the figure).

Table 3.3: The bandgaps for $Cd_{1-x}Zn_xSe$ nanorods calculated by different methods

Initial Cd^{2+}/Zn^{2+} molar ratio	Final products	E_{g1} [eV] (1)	E_{g2} [eV] (2)	E_{g3} [eV](3)
1 : 0	CdSe	1.74	1.74	1.75
1 : 1	$Cd_{0.65}Zn_{0.35}Se$	1.88	1.96	1.99
1 : 2	$Cd_{0.46}Zn_{0.54}Se$	2.03	2.12	2.07
1 : 4	$Cd_{0.39}Zn_{0.61}Se$	2.1	2.19	2.18
0 : 1	ZnSe	2.61	2.61	2.55

4.2. Photoconductivity

Figure 3.12a shows the photocurrent generation of $Cd_{1-x}Zn_xSe$ (x = 0, 0.35, 0.54, 0.61, 1) nanorods subjected to the on/off cycle of white light illumination. One can see that the nanorods can be reversibly switched between the low and the high conductivity state. As shown in the Figure 3.12a, a steady photocurrent was produced in CdSe, ZnSe and three $Cd_{1-x}Zn_xSe$ samples when the irradiation was switched on and the current returned approximately to the baseline when the light was switched off.

The on/off ratio, which is defined as the current under the irradiation over the dark current, is also presented in the Figure 3.12b as a function of the illuminated time. CdSe sample shows the highest on/off ratio (approximately 7.12), the next come to $Cd_{0.65}Zn_{0.35}Se$, $Cd_{0.46}Zn_{0.54}Se$, $Cd_{0.39}Zn_{0.61}Se$ samples with the on/off ratio of about 5.74, 2.20, 2.04, respectively; and the lowest one belongs to ZnSe (~1.46). As we know, the photocurrent derives mainly from electron-hole pair excited by incident light with energy larger than the bandgap, that is, only light with enough energy is able to induce a significant increase in current. In addition, energy of a phonon in excess of the semiconductor's bandgap ($h\upsilon > E_g$) is efficiently converted to heat through electron and hole interactions with the crystal lattice, resulting in larger electron and hole mobility and contributing a higher conductivity. In our experiment, the wavelength of the incident light is from 400 to 800 nm. The electron-hole pair of CdSe (bandgap of 1.74 eV) can be excited by the light with the wavelength less than 710 nm. It means that most of the incident light can be used to excite and mobilize electron and hole in CdSe nanorods, resulting in higher photoconductivity as compared to alloyed $Cd_{1-x}Zn_xSe$ (x = 0.35, 0.54, 0.61, 1.74 eV <bandgap< 2.61 eV) and ZnSe (bandgap of 2.61 eV).

On the other hand, the reaction rate in CdSe case is higher than three alloys and ZnSe as mentioned above. This produced more defects in CdSe nanorods which lead to the retardation of electron-hole recombination. Therefore, the photocurrent in CdSe is higher than the alloys and ZnSe.

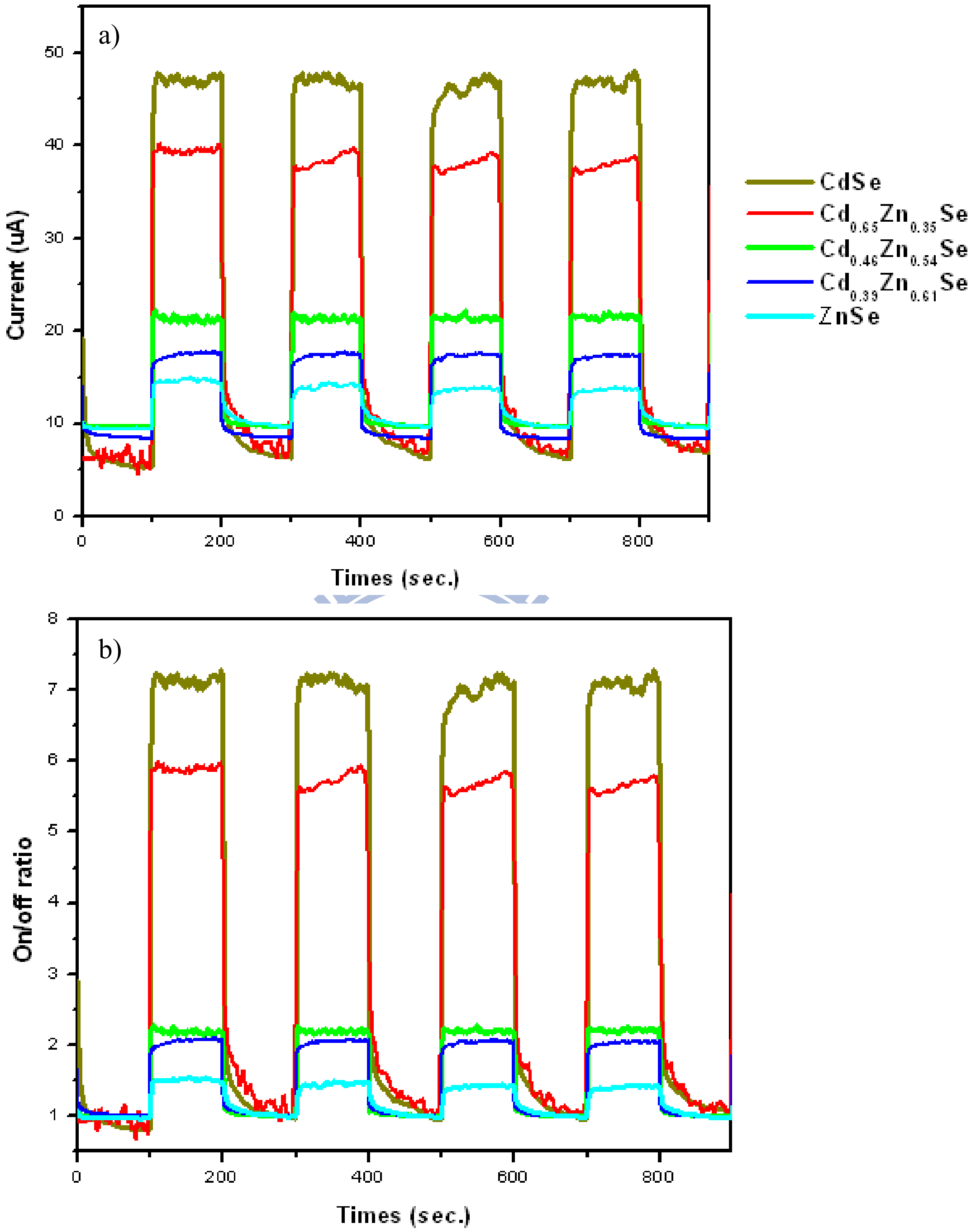

Figure 3.12: a) Photocurrent generation of CdSe, $Cd_{0.65}Zn_{0.35}Se$, $Cd_{0.46}Zn_{0.54}Se$, $Cd_{0.39}Zn_{0.61}Se$, and ZnSe nanorods. b) Plots of on/off ratio as a function of time for the five nanorod samples.

IV. CONCLUSIONS AND PERSPECTIVE

Overall, we have demonstrated the use of cation exchange as a general and effective approach to synthesize $Cd_{1-x}Zn_xSe$ nanorods. The mechanism of their formation were studied and discussed.

This work focused on the synthesis of $Cd_{1-x}Zn_xSe$ nanorods via the cation exchange between the Ag^+ in Ag_2Se and the M^{2+} (M = Cd, or Zn) in solution. All the products showed monodispersity in size, smooth surface, and rod-like shape. In these systems, the reaction of $Ag_2Se \rightarrow Cd_{1-x}Zn_xSe$ is intrinsically non-spontaneous at room temperature because of the large difference in solubility. As a result, the cation replacement relied on the use of TBP as a catalyst and elevation of temperature. Our results show that a topotactic relationiship between the anion sublattices was not a prerequisite for cation replacement, since ZnSe does not show any topotactic relationship with Ag_2Se.

$Cd_{1-x}Zn_xSe$ nanorods were synthesized and their photoconducting capability was demonstrated. $Cd_{1-x}Zn_xSe$ nanorods were found to be perfectly alloyed in the entire range of Zn composition we applied. Photocurrents dramatically decreased when the zinc composition increases in alloyed samples. In on-off switching operations, the CdSe sample was found to have better photoresponse than ZnSe and the alloyed ones. The present results demonstrate that $Cd_{1-x}Zn_xSe$ alloyed nanorods can be practically applicable to relevant photodetectors that may cover almost full range of visible spectrum of light extending from blue to red.

As a final note, it is feasible to use cation exchange reactions to significantly expand the scope of II-VI semiconductor nanorods, for example, PbSe nanorods. We expect that this method can be extended to synthesize high-quality alloyed nanorods of other materials.

V. REFERENCES

[1]. Mathew C. Beard and Randy J. Ellingson *Laser & Photonics Review* **2008**, 2, 377-399.

[2]. Unyong Jeong, Jong-Uk Kim, and Youman Xia *Nano lett.* **2005**, 5, 937-942.

[3]. Sasanka Deka, Alessandra Quarta, Maria Grazia Lupo, Andrea Falqui, Simona Boninelli, Cinzia Giannini, Giovanni Morello, Milena De Giorgi, Guglielmo Lanzazi, Corrado Spinella, Roberto Cingolani, Teresa Pellegrino, and Liberato Manna *J. Am. Chem. Soc.* **2009**, 131, 2948-2958.

[4]. Ken-Tye Yong, Jun Qian, Indrajit Roy, Hoon Hi Lee, Earl J. Bergey, Kenneth M. Tramposch, Sailing He, Mark T. Swihart, Anirban Maitra, and Paras N. Prasad *Nano Lett.* **2007**, 7, 761-765.

[5]. Ken-Tye Yong, Indrajit Roy, Haridas E. Pudavar, Earl J. Bergey, Kenneth M. Tramposch, Mark T. Swihart, and Paras N. Prasad *Adv. Matter.* **2008**, 20, 1412-1417.

[6]. Polina O. Anikeeva, Jonathan E. Halpert, Moungi G. Bawendi, and Vladimir Bulovic *Nano Lett.* **2009**, 9, 2532-2536.

[7]. Chao Xu and Eric Bakker *Anal. Chem.* **2007**, 79, 3716-3723.

[8]. Qingling Zhang, Suresh Gupta, Todd Emrick, and Thomas P. Russell *J. Am. Chem. Soc.* **2006**, 128, 3898-3899.

[9]. Qingling Zhang, Thomas P. Russell, and Todd Emrick *Chem. Mater.* **2007**, 19, 3712-3716.

[10]. Asit Baran Panda, Somobrata Acharya, Shlomo Efrima, and Yuval Golan *Langmuir* **2007**, 23, 765-770.

[11]. Donghuan Qin, Hong Tao, Yun Zhao, Linfeng Lan, Keith Chan and Yong Cao *Nanotechnology* **2008**, 19, 355201.

[13]. LeeAnn Kim, Polina O. Anikeeva, Seth A. Coe-Sullivan, Jonathan S. Steckel, Moungi G. Bawendi, and Vladimir Bulovic *Nano Lett.* **2008**, 8, 4513-4517.

[14]. Wenhao Liu, Hak Soo Choi, John P. Zimmer, Eiichi Tanaka, John V. Frangioni, and Moungi Bawendi *J. Am. Chem. Soc.* **2007**, 129, 14530-14531.

[15]. Hsiao-Sheng Chen, Chih-Wei Chen, Chun-Hsiung Wang, Feng-Ching Chu, Chih-Yu Chao, Chia-Cheng Kang, Pi-Tai Chou, and Yang-Fang Chen *J. Phys. Chem. C* **2010**, 114, 7995-7998.

[16]. Asit Baran Panda, Garry Glaspell, and M. Samy El-Shall *J. Am. Chem. Soc.* **2006**, 128, 2790-2791.

[17]. Qing Peng, Yajie Dong, Zhaoxiang Deng, and Yadong Li *Inorg. Chem.* **2002**, 41, 5249-5254.

[18]. Bonil Koo and Brian A. Korgel *Nano Lett.* **2008**, 8, 2490-2496.

[19]. Dmitri V. Talapin, Elena V. Shevchenko, Christopher B. Murray, Andreas Kornowski, Stephan Forster, and Horst Weller *J. Am. Chem. Soc.* **2004**, 126, 12984-12988.

[20]. Dmitri V. Talapin, James H. Nelson, Elena V. Shevchenko, Shaul Aloni, Bryce Sadtler, and A. Paul Alivisatos *Nano Lett.* **2007**, 7, 2951-2959.

[21]. Nishshanka N. Hewa-Kasakarage, Maria Kirsanova, Alexander Nemchinov, Nickolas Schmall, Patrick Z. El-Khoury, Alexander N. Tarnovsky, and Mikhail Zamkov *J. Am. Chem. Soc.* **2009**, 131, 1328-1334.

[22]. Jian-Ping Ge, Sheng Xu, Jing Zhuang, Xun Wang, Qing Peng, and Ya-Dong Li *Inorg. Chem.* **2006**, 45, 4922-4927.

[23]. Myriam Protière and Peter Reiss *Small* **2007**, 3, 399-403.

[24]. Steven A. Santangelo, Eric A. Hinds, Vladimir A. Vlaskin, Paul l. Archer, and Daniel R. Gamelin *J. Am. Chem. Soc.* **2007**, 129, 3973-3978.

[25]. Xinhua Zhong, Zhihua Zhang, Shuhua Liu, Mingyong Han, and Wolfgang Knoll *J. Phys. Chem. B* **2004**, 108, 15552-15559.

[26]. Fang-Chen Liu, Tian-Lu Cheng, Chien-Chih Shen, Wei-Lung Tseng, and Michael Y. Chiang *Langmuir* **2008**, 24, 2162-2167.

[27]. Xinhua Zhong, Mingyong-Han, Zhili Dong, Timothy J. White, and Wolfgang Knoll *J. Am. Chem. Soc.* **2003**, 125, 8589-8594.

[28]. LarissaDloczik; Rolf Könenkamp *Nano Lett.* **2003**, *3,* 651.

[29]. Dong Hee Son, Steven M. Hughes, Yadong Yin, A. Paul Alivisatos *Sciences* **2004**, 306, 1009-1012.

[30]. Geon Dae Moon, Sungwook Ko, Younan Xia, and Unyong Jeong *ACS NANO* **2010**, XXX, 000-000.

[31]. Unyong Jeong, Pedro H. C. Camargo, Young Hwan Lee, and Younam Xia *J. Matter. Chem.* **2006**, 16, 3893-3897.

[32]. Yungwon Park, Jaimei Zheng, Young-wook Jun, and A. Paul Alivisatos *J. Am. Chem. Soc.* **2009**, 131, 13943-13945.

[33]. Wei Zhu, Wenzhong Wang, and Jianlin Shi *J. Phys. Chem. B* **2006**, 110, 9785-9790.

[34]. Richard D. Robinson, Bryce Sadtler, Denis O. Demchenko, Can K. Erdonmez, Lin-Wang Wang, A. Paul Alivisatos *Science* **2007**, 317, 355-358.

[35]. Joseph M. Luther, Haimei Zheng, Bryce Sadtler, and A. Paul Alivisatos *J. Am. Chem. Soc.* **2009**, 131, 16851-16857.

[36]. Unyoung Jeong, Younan Xia, Yadong Yin *Chemical Physics Letters* **2005**, 416, 246-250.

[37]. Xinhua Zhong, Mingyong Han, Zhili Dong, Timothy J. White, and Wolfgang Knoll *J. Am. Chem. Soc.* **2003**, 125, 8589.

[38]. Y. S. Wang, P. John Thomas, and P. O'Brien *J. Phys. Chem. B* **2006**.

[39]. Saliha Ilican, Muhsin Zor, Yasemin Caglar, Mujdat Caglar *Optica Applicata* **2006**, XXXVI, 29-37.

[40]. Byron Gates, Yiying Wu, Yadong Yin, Peidong Yang, and Youman Xia *J. Am. Chem. Soc.* **2001**, 123, 11500-11501.